ORIGINAL ARTICLE

lajss.org© Latin American Journal of Solids and Structures

www.lajss.org

Bond Behavior of Auxetic Bars in Reinforced Concrete – A Numerical Study

Jesús Antonio García Sánchez[a*], Carolina Quintero Ramírez[a], Paulo Cesar Gonçalves[a], Oscar Javier Begambre[b]

[a]Universidade Federal de Itajubá, Campus Prof. José Rodrigues Seabra – Sede, Av. BPS, 1303, Itajubá – MG, Brasil. E-mail: jesus@unifei.edu.br, carolqr@unifei.edu.br, paulocg9@unifei.edu.br

[b]Universidad Industrial de Santander -UIS, Campus central, Bucaramanga, Colombia. E-mail: ojbegam@uis.edu.co

* Corresponding author

https://doi.org/10.1590/1679-78257917

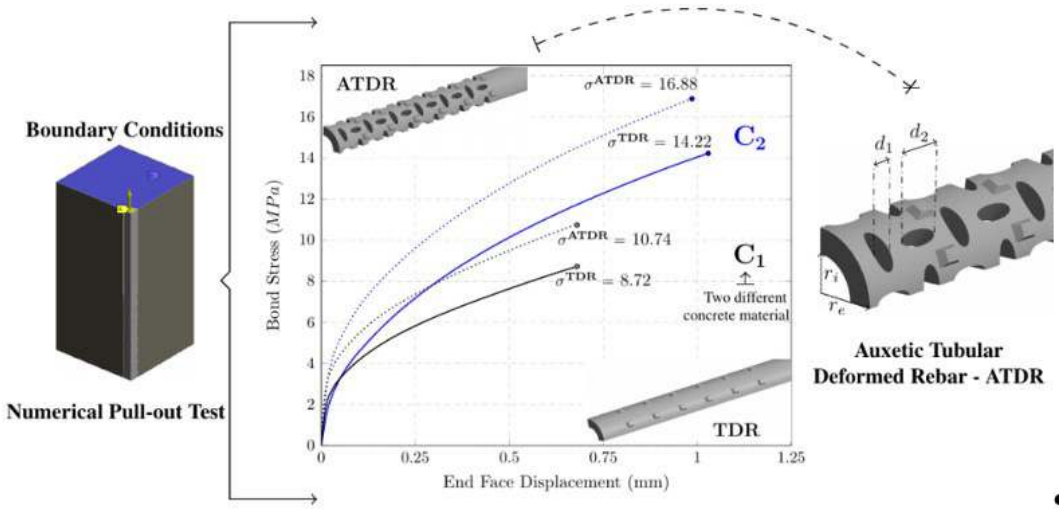
Abstract

The study aims to enhance the bonding strength in reinforced concrete using a novel Auxetic Tubular Deformed Rebar (ATDR). A high-resolution non-linear finite element model was developed to perform numerical analysis of pull-out tests (PoT). Two sets of numerical simulations were conducted: one to replicate the concrete behavior under compression and tension tests, and the other for PoT, validated with experimental and numerical data. Numerical tests utilized a microplane model with plasticity–damage, regularized by an implicit gradient. Auxetic geometry involves adding ellipsoidal orifices to the rebar surface. Comparing the behavior of ATDR with the conventional rebar, we observed an increase in the negative value of Poisson's ratio, resulting in higher normal and shear forces, enhancing adherence. This study presents the first comprehensive simulation of Auxetic Metamaterial Rebar in concrete, offering a promising approach to enhance bond strength. Further research, both numerical and experimental, is essential to assess Auxetic Reinforcement's mechanical behavior in diverse structural elements and load scenarios.

Keywords

Auxetic Metamaterials, Reinforced Concrete, Bond Strength, Numerical Pull-out Test.

Graphical Abstract



Received: November 11, 2023. In revised form: February 08, 2024. Accepted: February 21, 2024. Available online: March 01, 2024
https://doi.org/10.1590/1679-78257917

Latin American Journal of Solids and Structures. ISSN 1679-7825. Copyright © 2024. This is an Open Access article distributed under the terms of the Creative Commons Attribution License, which permits unrestricted use, distribution, and reproduction in any medium, provided the original work is properly cited.

1 INTRODUCTION

Auxetic Metamaterials (AMm) exhibit negative Poisson's ratios and are found in nature in substances such as zeolites, silicon dioxides, graphene and proteins (Li et al., 2017). Various geometric arrangements have been proposed to artificially achieve auxetic behavior, including chiral, honeycomb and origami cells (Li et al., 2017). In recent years, topology optimization has been utilizes to create 2D and 3D auxetic microstructures (Gao et al., 2019; Zhang and Khandelwal, 2019). However, further advancements are needed to make this technology practical and applicable in real-world civil engineering scenarios. In this context, most analytical and experimental studies reporting on AMm have focused on the microstructure (Fleck et al., 2010; Martinsson and Babuška, 2007). However, as mentioned in Li et al. (2017) and Zhang and Khandelwal (2019) the design of AMm that can be used as concrete reinforcement, (in this case, we called as auxetic bars metareinforcement) with non-linear characteristics, remains an open issue. To the best of the authors' knowledge, there is no analytical formulation available in the consulted literature to determine the mechanical properties of this type of concrete reinforcement. Furthermore, obtaining reinforced concrete with auxetic rebars presents a substantial technical challenge. To date, most research in concrete reinforcement has focused on explaining bond strength between reinforcement rebars/fibers and concrete from the perspective of chemical, frictional and geometric characteristics (e.g., bar diameter or rib area) (Tran et al., 2021; Miranda et al., 2021; De Maio et al., 2019). In contrast, there have been no studies analyzing the use of AMm as concrete reinforcement and their influence on the behavior of reinforcement bond strength. In a related context, Hou et al. (2018) conducted a comprehensive experimental study on panel sandwich composites reinforced with three 3D printed cores of auxetic lattices (re-entrant honeycomb, diamond lattice and conventional honeycomb). In a three-points bending cyclic low-velocity test carried out, the re-entrant honeycomb displayed a low peak reaction force and high-energy loss due to the negative Poisson's ratio. Regarding the design and experimental characterization of real 3D AMms, Ren, Shen, et al. (2018b) introduced twelve new auxetic nails (AN) with different geometries. The comparison of maximum compression and traction forces supported by AN and two non-auxetic nails, one with circular holes (CN) and the other solid (SN), demonstrated that the proposed AN did not consistently outperform CN and SN. According to Ren, Shen, et al. (2018b) three factors influenced the results obtained in the push-in and pull-out tests with AN: the roughness of the nails surface, the shape of the nail's holes, and the mechanical properties of the nail (some nails were partially auxetic) and the timber. However, they did observe an increase in the pull-out forces of some models of the tested AN compared to the pull-out test results of non-auxetic nails. This last result motivated us to search for AMm with high mechanical performance in pull-out tests, which could enhance adhesion between materials and, therefore, be utilized as concrete reinforcement elements.

Considering these issues and recognizing that AMm rebars could enhance adherence by increasing the normal force between concrete and AMm rebar, we present compelling numerical evidence suggesting that developing AMm rebar using macroscopic static non-linear finite element analysis (FEA) could be feasible. As previously mentioned in Brisotto, Bittencourt and Bessa (2012), there are three scales for analyzing classical concrete-steel bond strength through FEA: low resolution (1D); mid-resolution (3D), which can capture auxetic and bonding strength behavior but lacks rebar details; and the high-resolution scale (HRS), which can account for reinforcement geometry, such as ribs or holes. The HRS has been infrequently used due to its high computational cost and the scarcity of experimental data (Seok et al., 2020; Song et al., 2020; Brisotto et al., 2012). Furthermore, FEA must be complemented by appropriate constitutive models, and as indicate in Indriyantho et al. (Indriyantho, Zreid and Kaliske, 2019), the microplane (MP) constitutive model offers a powerful approach to model concrete behavior.

The pull-out test has been studied both numerically and experimentally in important studies (Liang et al., 2017; Concha and Oreta, 2021; Liang et al., 2021; Tang, 2015; Arslan and Pul, 2020; Friedrich and Wang, 2016). The adhesion phenomena occurring at the interface between concrete and reinforcement at the mid-resolution (3D) level are presented in the literature (Lundgren and Gylltoft, 2000; Lundgren, 2005a; Lundgren, 2005b; Salem and Maekawa, 2004; Erfanian and Elwi, 2019). The analysis at the HRS scale can be found in Seok (2019). Benin et al. (2013) and Benin et al. (2014) explored models that account for the discontinuity in the connection between the rebar and concrete during pullout tests. They conducted both numerical and experimental tests to analyze the nonlinear mechanical behavior observed in bond strength and concrete cracking. Various models of bond behavior and concrete cracking were employed in the numerical simulations, and the obtained results were subsequently compared with the experimental data.

In recent years, scientific studies have highlighted the significance of incorporating metamaterials as innovative technology in concrete. Among the notable research contributions are those by Mitchell et al. (2014), Barri et al. (2022), Mitchell, Pandolfi and Ortiz (2015), Ramírez et al. (2022), Zhong et al. (2022), Gupta et al. (2023) and many others.

In this context, creating a reliable and reproducible FEA that accurately represents classical pull-out studies and the performance of AMm rebars in these tests is a fundamental challenge. Recently, an sophisticated HRS FEA analysis, utilizing ABAQUS®, was employed successfully by Song et al. (2020) to access the design of a novel cable anchorage.

This analysis included considerations of bonding strength and friction between concrete and cables. In the work of Qasem et al. (2020), the authors developed and calibrated a quasi-static non-linear HRS finite element model based on cohesive elements to describe the bond-slip behavior of ultra-high-performance concrete reinforced with carbon fiber polymer rebars. Their model, which consisted of $147{,}008$ 3D quadratic solid elements, produced realistic results that closely matched experimental data. Additionally, Seok et al. (2020) conducted a comprehensive HRS FEA pull-out test using ABAQUS®. The study presented simulations of the interfacial bond strength between concrete and steel and the non-linear material response of the concrete caused by interactions with the ribbed surface. Two concrete constitutive models were evaluated, namely the concrete damaged-plasticity (CDP) model and the CDP Model 2 (CDPM2). The latter model can simulate static non-linear responses under varying confining pressures and various multiaxial stress states. In their studies, Seok et al. (2020) reported that using CDPM2 accurately simulates both splitting and pull-out failure for the specimens under investigation, with and without confinement, respectively. Li et al. (2013) conducted a comprehensive study to validate the MP M4L model. The predictive capacity of M4L was thoroughly tested, and the authors demonstrated its accurate description of the material response of concrete under multiaxial loadings in non-linear structural analysis. Based on these results, in this work incorporates the CDP, CDPM2 and M4L, constitutive models, which are based on finite strain (Seok et al., 2020; Li et al., 2013; Indriyantho et al., 2019), to propose a macroscopic HRS static non-linear Finite Element Analysis for simulating bond stress-slip interactions in pull-out tests involving AMm rebars.

This work has a dual purpose: firstly, to asses a new Auxetic Tubular Deformed Rebar (ATDR) and secondly, to offer substantial numerical evidence supporting the possibility of developing a novel AMm reinforcement element for concrete structures that either matches or surpasses the performance of conventional ones. To achieve this, we have examined three numerical scenarios for pull-out tests on cylindrical and prismatic concrete specimens, utilizing the following reinforcement types: conventional rebars, partially ribbed Tubular Deformed Rebar (TDR), and ATDR. All simulations were conducted using ANSYS® (2020).

In this paper, the simulations are divided in two sections: validation and proposed examples (section 2), and the results are presented in section 3. In the calibration model example (section 2), which involves concrete compression and tension test, the MP damage theory is employed. It utilized a combined plasticity–damage model that is enhanced by an implicit gradient. The plasticity component introduces a smooth three-surface cap yield function, and the results are compared with both numerical and experimental data. The first example for pull-out numerical testing, known as the validation model, aims to replicate the behavior of a pull-out test using the MP damage model. The second pull-out numerical test example serves as a reference model -TDR, where a partially ribbed tube is utilized as reinforcement. This geometric configuration was chosen to compare to compare its behavior with the proposed geometry. Finally, the third pull-out numerical test example presented the proposed model – ATDR. In this case, the reinforcement of the second pull-out test was modified by introducing an auxetic reinforcement (metareinforcement). This modification allows to identify the effects of the negative Poisson's ratio on the mechanical behavior of the reinforced concrete.

1.1 Auxetic Metamaterials

Metamaterials (Mms) are often described as periodic arrangements organized into blocks that possess properties and functionalities differing and enhancing those of the constituent materials (Bertoldi et al., 2017; Xianglong et al., 2018; Guevara-Corzo et al., 2022; Jagiello and Muñoz-Rojas, 2021). Several studies can be found in the literature that explores appications in engineering and structural design (Fraternali et al., 2015; Gonçalves Salsa Junior et al., 2022; Comi and Driemeier, 2018; Rodrigues et al., 2019; between others). Following Bertoldi et al. (2017), deformation can be one of the properties that can be controlled using Mms. This enables the manipulation of the physical behaviors that were previously considered impossible or unusual in natural materials. Such behaviors may include: exceptional strength and stiffness-to-weight ratios; excellent strain recoverability; very soft or very stiff deformation modes; auxetic behavior; phononic band-gaps; sound control ability; negative effective mass density; negative effective stiffness; negative effective refraction index; superlens behavior; and/or localized confined waves (Fraternali et al., 2015).

A type of Mms with direct applications in reinforced concrete is known as AMm, which exhibits a negative Poisson's ratio. Ren, Das, et al. (2018a) and Ren, Shen, et al. (2018b) describe in their work that AMm has a counterintuitive effect: when a structure is subjected to tension (resulting in positive deformation), its lateral deformation also becomes positive (see Figure 1b). Ren, Shen, et al. (2018b) employed an auxetic geometry comprising alternating elliptical hollows in their work. This geometry was applied in AN to enhance the mechanical functionality of nails (see Figure 1). Other studies have utilized the concept of Mms to design surface morphology and manipulate the roughness, improving the mechanical behavior of reinforced concrete and composite materials (Farina et al., 2016a, b; Fabbrocino et al., 2016).

The AMms have potential for multiple applications; however, their industrial fabrication remains a challenge to be overcome, considering that the Mms area is a novelty in engineering. Nevertheless, these limitations cannot restrict the advances in research in this area, as it has demonstrated its potential in fields such as medicine and various types of engineering. To better understand the fabrication process of AMms and their challenges, it is recommended to study the works of Luo et al. (2021) and Zhang et al. (2020), where similar structures to those proposed in this paper are addressed.

Hence, employing AMm as a rebar in concrete elements has the potential to enhance the bond between the concrete matrix and reinforcement. We have applied auxetic geometry initially proposed by Ren, Das, et al. (2018a) and Ren, Shen, et al. (2018b) in the design of the ATDR. Our aim is to enhance the adherence by amplifying the normal pressure on the interface surface through the positive deformation achieved with the utilization of AMm.

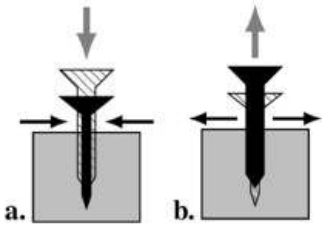


Figure 1. Illustration of auxeticity: (a) push-in; (b) pull-out (pattern and black color represent the configurations before and after deformation, respectively.) -Adapted from. (Ren, Das, et al., 2018a) *and* (Ren, Shen, et al., 2018b)

1.2 Concrete Constitutive model – Microplane MP

Continuous damage mechanics is the classic approach used to locally describe the evolution of distributed damage phenomena caused by microcracks and voids. I incorporate the concepts of effective stress and strain equivalence, with its formulation considering the reduction of the cross-sectional area during the material's tensile load transmission. However, the multiaxial generalization of continuous damage mechanics remains largely unresolved challenge, involving complex numerical implementations of stresses in random spatial directions (Carol et al., 1991). One strategy in addressing multiaxial continuum damage model theories is the MP model. One of the model's key advantages is that it focusses primarily in stress-strain relationships ate the MP level, eliminating the need to meet tensor invariance requirements, which often pose significant difficulties in constitutive modeling (Bazant, 1984; Bazant and Prat, 1989). This flexibility enables the model to handle problems related to materials exhibiting inelastic responses due to localized micro-cracks, such as those found in concrete. In processes involving crack growth, quasi-brittle materials often exhibit a thin layer or process zone ahead of the crack. This zone experiences significant damage, leading to stiffness degradation, a substantial increase in strain and a decrease in peak stress due to material softening. Therefore, coupling damage with plasticity is essential for accurate constitutive modeling of concrete (Zreid and Kaliske, 2016a). In this context, the MP model can incorporate damage by considering the degradation of stiffness in a directional manner, within individual planes with failure potential. This approach results in macroscopic anisotropic damage (Zreid and Kaliske, 2018; Seok et al., 2020).

The MP concept is appealing due to its capacity to naturally and simply describe the initial anisotropic behavior and the progression of damage in a material (Leukart and Ramm, 2003).

In the formulation of the MP, it is necessary to predict coupling restrictions that establish a relationship between the behavior of all microplanes and the macroscopic behavior level. The imposition of kinematic constraints leads to the formulation of the macroscopic stress tensor as an integral along the spherical surface, representing the normal and shear stresses in each microplane. The inclusion of the deformation softening effect in the formulation addressed complex aspects of the triaxial behavior, particularly in nearly brittle materials and certain composites. Kinematic constraints have been shown to mathematically describe typical results observed in concrete tests related to microcrack states (Bazant, 1984; Bazant et al., 1984; Bazant and Oh, 1985; Bazant and Pijaudier-Cabot, 1989; Bazant and Ozbolt, 1991; Carol et al., 1991).

Originally conceived to capture plasticity parameters and damage responses in the formulation for quasi-brittle materials (Brocca and Bažant, 2000; Kuhl et al., 2000), the constitutive laws in the MP formulation have advanced from an alternative approach based on volumetric-deviation division associated with the Drucker-Prager flow function (Leukart and Ramm, 2006). The MP constitutive formulation approach considers thermodynamic consistency, ensuring the association between the load cycle sequence and energy dissipation (Zreid and Kaliske, 2018) (Zreid and Kaliske, 2016b). In this context, the macroscopic Helmholtz thermodynamic free energy (ψ^{mac}) is obtained as the integral of the free energies of the microplane (ψ^{mic}) in all orientations on spherical surface planes, as expressed in the following equation,

$$\psi^{mac} = \frac{3}{4\pi}\int_{\Omega}\psi^{mic}d\Omega \tag{1}$$

The free energy at the microplane level is expressed as a function of plasticity in terms of isotropic hardening, defined as:

$$\psi^{mic} = \frac{1}{2}K^{mic}\left(\varepsilon_V - \varepsilon_V^{pl}\right)^2 + G^{mic}\left(\varepsilon_D - \varepsilon_D^{pl}\right).\left(\varepsilon_D - \varepsilon_D^{pl}\right) + \frac{1}{2}H_K^{mic}{}^2, \tag{2}$$

here, ε_V and ε_D represent the volumetric and deviatoric MP deformation, respectively. The superscript pl indicates the plastic part, and K^{mic} and G^{mic} are elastic parameter of the MP related to the Bulk and shear modulli, respectively. Additionally, H_K represents the hardening stiffness, and k^{mic} is a hardening variable (Zreid and Kaliske, 2018).

The classical modeling of the softening-by-strain phenomenon, particularly in the post-peak region of the concrete stress-strain curve, presents significant challenges. These challenges include a sensitive instability in the computational model mesh, primarily due to the presence of a thin layer ahead of the fracture during the crack propagation process. To address these issues, various nonlocal formulations incorporating different gradient types have been developed to efficiently account for microstructural effects within classical continuum models (Schreter et al., 2018). In the context of the evolution of the CDP model, the CDPM2 model emerges as promising concrete model. It has demonstrated remarkable capabilities in simulating nonlinear responses under static and dynamic multiaxial stress conditions, encompassing various ranges of confining pressures.

To address issues related to localized deformation, the method of regularizing the numerical model through the implicit gradient is employed. This approach helps eliminate mesh sensitivity and numerical instabilities. As a result, the MP formulation has gained popularity for describing quasi-brittle materials. It offers computationally efficiency surpassing that of conventional models (Leukart and Ramm, 2006; Grassl and Jirásek, 2006a; Zreid and Kaliske, 2016b; Zreid and Kaliske, 2018; Steinke et al., 2017; Schreter et al., 2018; Indriyantho et al., 2020).

In the MP model, the variable governing local damage is substituted with a linear combination of both local and non-local damage variables, with the inclusion of the on-local numerical parameter m. This approach was observed in the results obtained from the formulation of the plasticity model coupled with regularized non-local damage for concrete. When $m \geq 1$, it indicates well-distributed local plastic deformations and uniformity of damage (Grassl and Jirásek, 2006b). Another critical parameter whitin the numerical formulation of the model is the non-local interaction interval, denoted as c. This parameter is directly related to the characteristic length parameter l of quasi-brittle materials. It governs the minimum possible width of a damage zone resulting from deformation softening in non-local continuous formulations. Essenctially, it serves a limiting factor to prevent the damage zone from located whitin a zero volume region (Bazant and Pijaudier-Cabot, 1989).

The MP model utilized in the computational formulation of finite elements within this work incorporates the modified Drucker-Prager plasticity-damage criterion. This criterion's function has been augmented with a cap for both compression and traction regions to capture intricate triaxial behavior of concrete through a yield function. As demonstrated by Zreid and Kaliske (2018), the adoption of a smooth cap yield function featuring three MP surfaces represents a robust strategy to overcoming the singularity issues encountered in the tangent terms on the non-smooth yield surfaces, particularly within the corner region. Such singularities can lead to numerical instability.

Utilizing the volumetric-deviatoric ($V-D$) split, the Drucker–Prager yield function is formulated based on three stress states invariants, as showed in Figure 2. The model is founded on the theory developed by Schwer and Murray (1994) and can be expressed as:

$$f^{mic}\left(\sigma_D^e, \sigma_V^e, \kappa\right) = \frac{3}{2}\sigma_D^e.\sigma_D^e - f_1^2\left(\sigma_V^e, \kappa\right).f_c\left(\sigma_V^e, \kappa\right).f_t\left(\sigma_V^e, \kappa\right) \tag{3}$$

The Drucker–Prager hardened yield surface is represented as

$$f_1 = \sigma_0 - \alpha\sigma_V^e + f_h(\kappa), \tag{4}$$

here σ_0 represent the initial yield stress, σ_V^e denotes the volumetric MP effective stress, α is the friction coefficient, and $f_h(\kappa) = D\kappa$ represents the linear hardening function with D as the constant hardening variable.

The functions f_c and f_t in Eq. 3 represent the compression and tension caps, respectively, and are defined as:

$$f_c = 1 - H_c\left(\sigma_V^C - \sigma_V^e\right).\frac{\left(\sigma_V^e - \sigma_V^C\right)^2}{X^2},\ f_t = 1 - H_t\left(\sigma_V^e - \sigma_V^T\right).\frac{\left(\sigma_V^e - \sigma_V^T\right)^2}{\left(T - \sigma_V^T\right)}, \tag{5}$$

here, σ_V^C and σ_V^e are geometric quantities of the smooth three-surface MP cap (Figure 2), and H_c and H_t are Heaviside functions (Zreid and Kaliske, 2018).

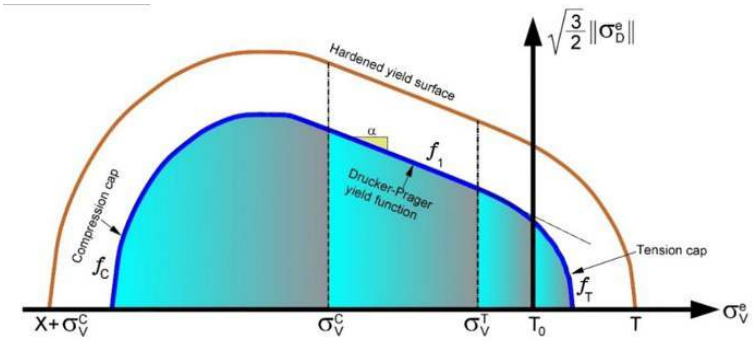


Figure 2. Smooth three surface MP cap yield function.

There is a parameter named R, which represents the ratio between the major to the minor axes of the cap, is obtained as:

$$R = \frac{X_0}{f_1 \sigma_V^C} \tag{6}$$

According to Lee and Fenves (1998), the progression of damage varies significantly between compression and tension in quasi-brittle element. In the case of concrete, it exhibits greater susceptibility to tension, initiating the softening process immediately after surpassing the elastic limit. Concersely, in compression, a certain degree of hardening is observed before the potential for softening. Additionally, durong the transition from tension to compression, there is a recovery of the stiffness lost during the cracking process in tension, attributed to the closure of the cracks. In this context, the damage formulation is segmented into the compression and tension parts, as outlined below,

$$1 - d^{mic} = \left(1 - d_c^{mic}\right).\left(1 - r_w.d_t^{mic}\right) \tag{7}$$

The tensile and compression components of the damage evolution law are expressed as:

$$\begin{aligned} d_t^{mic} &= 1 - exp\left(-\beta_t.\gamma_t^{mic}\right), \\ d_c^{mic} &= 1 - exp\left(-\beta_c.\gamma_c^{mic}\right), \end{aligned} \tag{8}$$

here, β_t and β_c represent parameters associated with the tensile and compression components, respectively, while γ_t^{mic} and γ_c^{mic} denote the corresponding damage variables.

The parameters m and c are the nonlocal parameters. The parameter m can be regarded as a numerical parameter, where any value greater than 1 will serve to regularize the solution. Meanwhile, the gradient parameter c will govern the extent of nonlocal interaction (Zreid and Kaliske, 2018) (Xenos et al., 2015).

Lastly, the numerical parameters required to define the MP model (E ,ν,f_{uc}, f_{bc}, R_t, D, σ_{Vc}, R, γ_{t0}, γ_{c0}, β_t, β_c, c and m) are presented in Table 1,Table 2 and Table 3. For additional information regarding these parameters, refer to Zreid and Kaliske (2018).

It is essential to emphasize that the primarily objective of this study is to examine the bond strength between concrete and a novel ATDR, rather than delving into the development of an entirely new concrete model. In this context, the comparison of results obtained through the FEM MP model with those derived from the CDP model serves the purpose of validating the proposed numerical simulation.

2 Numerical Simulations - Models

To illustrate the variation in adherence force between the concrete and an AMm rebar, a methodology has been developed utilizing two sets of geometrically and plastically non-linear HRS FEA numerical simulations, as depicted in Figure 3. Given that these are numerical simulations, it was necessary to first validate them before employing the model in simulations comparing the Pull-out of the auxetic bar with that of the non-auxetic bar. Thus, the first two types of simulations (i - Concrete compression and tension tests, and ii - Pull-out - validation HRS FEA model) seek to demonstrate that the plasticity-damage MP model adequaly captures the behavior of concrete obtainded in varios experimental test.

The first set (Concrete compression and tension test) utilizes the plasticity-damage MP model to verify whether the numerical simulations accurately replicate concrete behavior inder compression and tension loads. The data used for the concrete in the MP model for this first dataset are based on the information reported in the works of Seok et al. (2020) and Kupfer et al. (1969), with the remaining data calibrate according to methodologies recommended in the works of Zreid and Kaliske (2018), Jiang and Zhao (2015) and Xenos et al. (2015).

The second set includes examples of numerical Pull-out tests, convering validation models (Validation HRS FEA model – with conventional reinforcement bar), reference models (Pull-out HRS FEA models – with tubular deformed reinforcement bar – TDR), and proposed models (Pull-out HRS FEA models – with auxetic tubular deformed reinforcement bar – ATDR). Initially, in this set, a simulation for validation was performed (Pull-out Validation HRS FEA model), which utilizes the plasticity-damage MP model to reproduce the results of the Pull-out experiment, both numerical and experiental, of a convectional reinforcement bar reported in Seok et al. (2020) and Seok (2019). This type of validation is necessary as it demonstrates that the MP with plasticity-damage effectively captures the desired behavior in the Pull-out test, which will also be used to verify the potential improvement when using the auxetic bar. This MP model utilizes concrete data partly reported by Seok et al. (2020) and Seok (2019), with the remaining data calibrated according to methodologies recommended in the works of Zreid and Kaliske (2018), Jiang and Zhao (2015) and Xenos et al. (2015).

Finally, in the second type of Pull-out simulations, the numerical Pull-out test is performed with the auxetic bar (ATDR) and compared with the numerical Pull-ut test with the non-auxetic bar (TDR), serving as a reference. The data for the concrete in the MP model for this latter type of tests are based on those reported in Zreid and Kaliske (2018). This approach was necessary to verify the potential gain in reinforcement bar strength due to the auxetic behavior in thePull-out test.

All numerical examples are conducted as static structural analyses using the commercial software ANSYS® (2020). The constitutive and damage model utilized for the concrete is the MP. Mesh convergence analyses were conducted for all models.

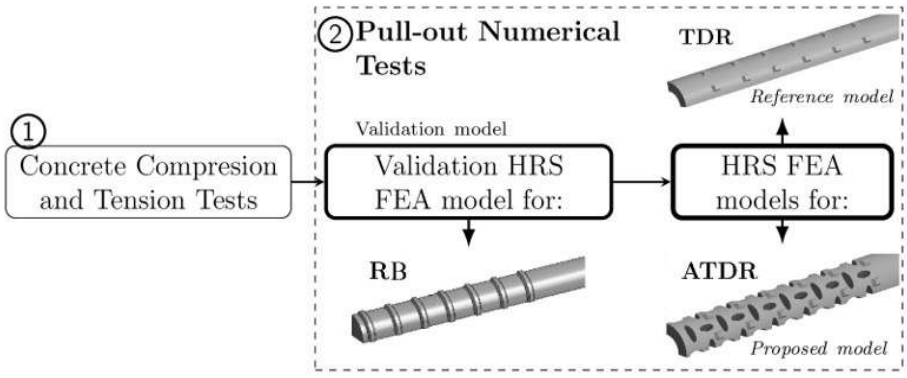


Figure 3. Fluxogram of models used in methodology.

2.1 Concrete Compression and Tension Tests

This section aims to validate the behavior of concrete through uniaxial compression and tension tests. In the compression test, a cylindrical specimen with $200\ mm$ length and a radius of $150\ mm$, Figure 4, was employed. The input parameters for the MP model (M1) can be found in Table 1. A uniaxial uniform displacement of $-1.5\ mm$ was applied to the top face, while the bottom face was restricted to vertical displacement. For the tension test, a specimen depicted in Figure 5, measuring $50\ mm \times 50\ mm \times 250\ mm$ in size, was utilized. The parameters of MP model (M2) can be found in Table 1. A positive uniaxial uniform displacement $\overline{U}$ was applied to the top face, while the bottom face was restricted to vertical displacement (Figure 5.). To reduce computational costs, two planes of symmetry were employed.

In Figure 4 and Figure 5 we compared our simulation (FEM MP) with the data reported by Seok et al. (2020) (CDPM2 and CDP), and with the experimental data of Kupfer et al. (1969) (Exp). According to the literature-data, the responses from FEM MP simulations exhibit a similar behavior. Figure 5 demonstrates that the results of the models closely align in the ascending portion of the stress-strain curve, up to the point of reaching the concrete tensile strength. In this segment, the material behaves in an almost linear manner. Upon reaching the maximum tensile strength, microcracks begin to develop, resulting in the subsequent softening of the material. Variations in the softening responses can be observed among the models. It is crucial to emphasize that after the stress peak, the concrete's tensile behavior becomes non-linear due to the formation of a region comprising micro-fractured material. Therefore, it is imperative for the FEM model to replicate the non-linearity of concrete under various multiaxial stress states and exhibit better agreement with the results of experimental tests. The results presented in the stress-strain curve of the FEM MP model reveal an enhanced alignment with the experimental curve (Exp) when compared to the other models in terms of non-linearity.

Table 1. Parameters of MP model for compression (M1) and tension (M2) numerical test.

Id Model	E [MPa]	ν	f_{uc} [MPa]	f_{bc} [MPa]	f_{ut} [MPa]	R_t	D [MPa]	σ_v^c [MPa]	R	γ_{t0}	γ_{c0}	β_t	β_c	c [mm^2]	m
M1	28000	0.2	28	$1.15f_{uc}$	3.4	1	8E4	-32	2	0	$5E-5$	3500	2000	1000	2.5
M2			40		3.7	2		-40			$8E-5$	10000		500	

E: elastic modulus of concrete, MPa. $\boldsymbol{\nu}$: Poisson's ratio. $\boldsymbol{f_{uc}}$: Uniaxial compressive strength, MPa. $\boldsymbol{f_{bc}}$: biaxial compressive strength, MPa. $\boldsymbol{f_{ut}}$: Uniaxial tensile strength, MPa. $\boldsymbol{R_t}$: Tension cap hardenin constant. **D**: hardenin material constant**,** MPa. $\boldsymbol{\sigma_v^c}$: Compression cap, MPa. **R**: ratio between the major and minor axes of the cap. $\boldsymbol{\gamma_{t0}}$, $\boldsymbol{\gamma_{c0}}$: tension and compression damagte thresholds. $\boldsymbol{\beta_t}$, $\boldsymbol{\beta_c}$: tensión and compression damage evolution constants. **c**: nonlocal interacion range parameter, mm² . **m**: over-nonlocal averaging parameter

2.2 Pull-out Numerical Tests

This section focuses on the development of numerical pull-out tests. Initially, a validation HRS FEA model for the numerical simulations was conducted and compared with literature results (Seok et al., 2020; Seok, 2019). Subsequently, HRS FEA models for TDR and ATDR with discontinuous ribs were introduced, and their numerical behavior was examined.

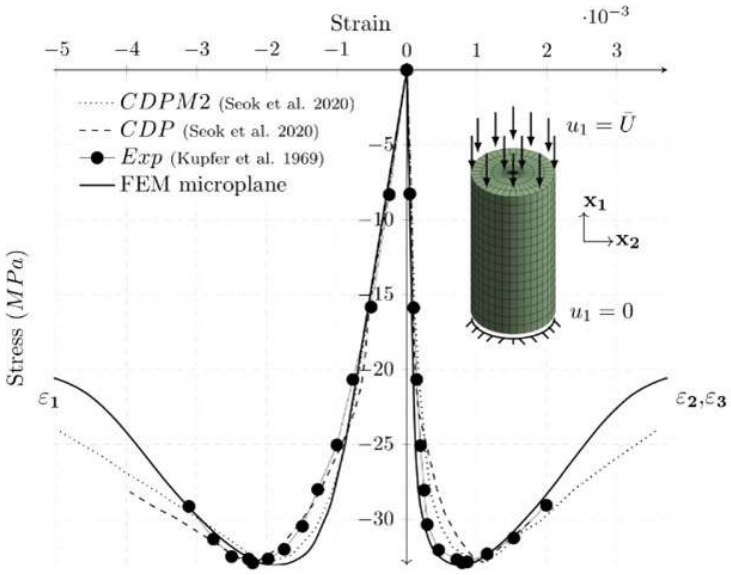


Figure 4. Stress vs. Strain of Compression test.

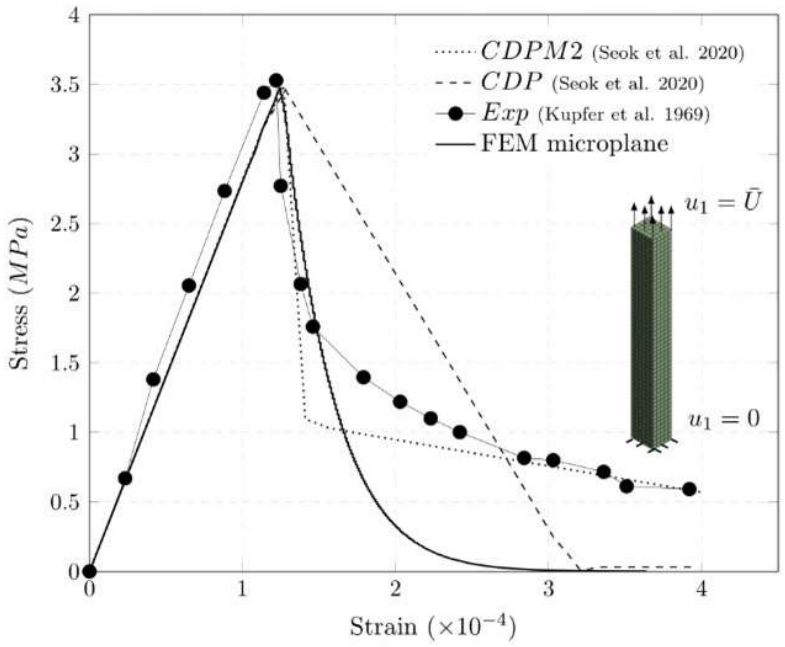


Figure 5. Stress vs. Strain – tension test.

The performance of TDR and ATDR models was compared to assess the variation in bonding strength. Identical values for the geometrical and material parameters were employed in both models. The sole distinction between the models lies in the utilization of alternating elliptical holes in the ATDR model. The proposed models were subjected with two different sets of concrete material properties, denoted as C1 and C2, as specified in Table 2 and Table 3.

The numerical pull-out tests were conducted as geometrically and plastically non-linear static problems. The pull-out specimen consists of a concrete block and ribbed rebar, as illustrated in Figure 6 to Figure 9. The concrete block measures $200\ mm \times 200\ mm \times 200\ mm$. The rebar, in all models, possesses an external diameter of $20\ mm$, while the tubular rebars feature an internal diameter of $12\ mm$. The specimens comprise a bonded region where the rebar makes contact with the concrete block and an unbonded region where the concrete block has a cylindrical hollow with a diameter larger than that of the rebar. The length of the bonded region, in the lateral view, is $100\ mm$.

As depicted in Figure 6, a displacement was applied at the end of the rebar. One face of the concrete prism was restricted in the same direction as the applied displacement. Two planes of symmetry were taken into account, simulating only a quarter of the concrete block and the rebar. The contact between the rebar was treated as frictional, with a frictional coefficient of 0.5.

Considering stress concentration aspects, the following recommendations were followed to prevent artificially stress in all strucutural finite element models: loading and contraints were applied on a single face, sharp corners were avoided, and primary results were analyzed in the concrete-reinforcement steel contact region. Regarding mesh and its configuration, two types of control, refinement, and quality, were applied for all models. Refinement was conducted to achieve stress convergence. The Jacobian ratio (JR) was used as the mesh quality criterion, varying between 0 for poor-quality elements and 1 for elements with optimal quality (ANSYS Inc., 2020). For the compression simulation, a flat structured mesh was utilized with CPT213 elements in Quad8 form (considering axisymmetric geometry) (ANSYS Inc., 2020), with a maximum size of $18.75\ mm$, and all elments had a $JR = 1.0$. Similarly, for the tension simulation, a structured mesh was employed, but with solid CPT217 elements in Hex20 form (ANSYS Inc., 2020), with a maximum size of $5\ mm$, and all elements had a $JR = 1.0$. For the Pull-out simulations, parameters were standardized for all numerical models, including face refinement for local mesh controls and stress analysis (to idenrify highly stresses areas). All Pull-out meshes were adaptative type and utilized solid CPT217 elements in Tet10 tetrahedral form (ANSYS Inc., 2020). Refinement measures included body-sizing of $2\ mm$ for reinforcement bars, a face-sizing of $2\ mm$ at the contact interfaces between reinforcement and concrete, with a smooth transition in element size configuration, and mesh resolution set to 3 (maximum of 7). The minimum JR of the TDR and ATDR models is greater thatn 0.55; specifically, for the TDR model, 89.54% of its elements have a $JR = 0.783$, 10.4% have a $JR = 0.928$, and 0.06% have a $JR = 0.639$. The ATDR model has 99.7% of tis elements with a $JR = 0.881$ and 0.3% with a $JR = 0.552$.

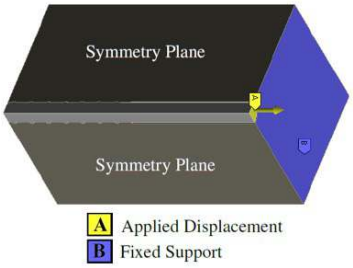


Figure 6. Pull-out test, boundary conditions.

2.2.1 Validation Model – Reinforcement Bar (RB)

A numerical pull-out test conducted to obtain the mechanical response of a convectional reinforced concrete structure, validating the employed numerical methodology. The acquired data were then compared with numerical and experimental data from the literature (Seok et al., 2020; Seok, 2019).

The material properties of concrete and structural steel are outlined in Table 2. In Figure 7, a three-dimensional view of the model along with finite element mesh details for the rebar is presented.

2.2.2 Reference Model - Tubular Deformed Rebar (TDR)

The TDR model, corresponding to the tubular rebar, was constructed using carbon epoxy material, and its properties are summarized in Table 3. In Figure 8, a three-dimensional view of the model is presented, along with details of the rebar and finite element mesh. The rebar has 20 mm and 12 mm of r_e and r_i, respectively. The rib dimensions are as follows: $l_1 = 2.8\ mm$, $l_2 = 4\ mm$, $l_3 = 14.69\ mm$, $l_4 = 11.68\ mm$, $h = 1.5\ mm$ and $n = 2\ mm$.

Table 2. Parameters of MP model (M3) and of structural steel for reinforcement bars (RB) for pull-out test for validation.

Id Model	E [MPa]	ν	f_{uc} [MPa]	f_{bc} [MPa]	f_{ut} [MPa]	R_t	D [MPa]	σ_v^c [MPa]	R	γ_{t0}	γ_{c0}	β_t	β_c	c [mm^2]	m
M3	26700	0.2	42.7	$1.15f_{uc}$	3.4	1	$1E4$	-18	2	0	$2E-6$	4000	2500	500	2.5
RB	$2E5$	0.3													

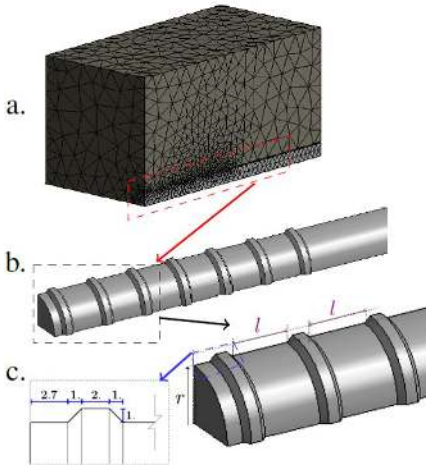


Figure 7. Geometrical model of pull-out test – validation example a) Model - 3D mesh b) Conventional rebar - 3D) Dimensions of rebar ribs in mm.

Table 3. Parameters of MP model for compression numerical test for concrete C1 and C2; and of Carbon Epoxy (CE).

Id Model	E [MPa]	ν	f_{uc} [MPa]	f_{bc} [MPa]	f_{ut} [MPa]	R_t	D [MPa]	σ_v^c [MPa]	R	γ_{t0}	γ_{c0}	β_t	β_c	c [mm^2]	m
C1	26700	0.2	28	$1.15f_{uc}$	2.8	1	$1E4$	-18	2	0	$5E-5$	4000	2500	500	2.5
C2			42.7		3.4			-32				3500	2000	1000	
CE	12400	0.2	2600												

2.2.3 Proposed Model - Auxetic Tubular Deformed Rebar (ATDR)

An innovative geometry was introduced for the rebar, featuring periodically alternating elliptical holes based on the concept of Mm. This geometry exhibits an auxetic behavior due to its negative Poisson's ratio. Consequently, when the rebar is subjected to tension, the radial displacement is positive, as demonstrated in section 3.

Figure 9 presents a three-dimensional view of the model under consideration, showcasing details of the rebar and finite element mesh. The rebar was also modeled using carbon epoxy material, and its properties are summarized in Table 3. The rebar features 20 mm and 12 mm of external and internal diameter, respectively. The ellipses on the rebar have dimensions of $d_1 = 3{,}28\ mm$ and $d_2 = 6{,}45\ mm$ for the minor and major axes, respectively. The rib dimensions of the rebar are the identical to those of the TDR model.

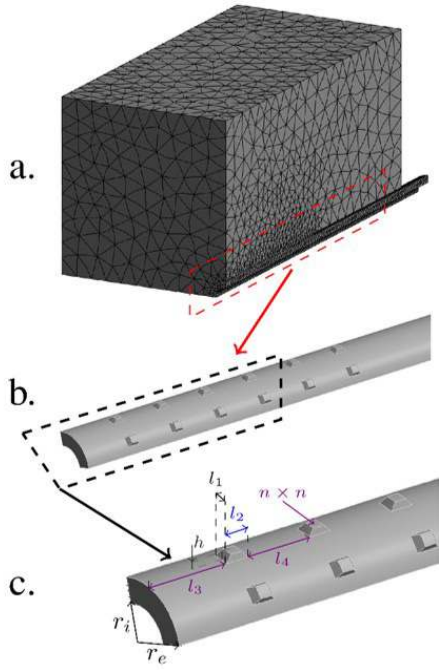


Figure 8. Geometrical model of pull-out test – reference example a) 3D view b) 3D bar - TDR c) Dimensions

3 Numerical Results – Pull-out

For all models presented in section 3, the following results are displayed: Bond stress - End displacement curve, results on the contact surface (Frictional stress and Pressure), and radial displacement.

The Bond stress - End displacement curve is generated following a procedure similar to that of Seok et al. (2020) and Seok (2019). Specifically, the bond stress is computed as the ratio of the applied force (the reaction force in the displacement boundary condition) to the contact area between concrete and the rebar. In the case of the ATDR geometry, the areas of elliptical holes are subtracted from the contact surface. The end displacement value corresponds to the movement of the rear face of the reinforcement, which is opposite to the face where the boundary condition is applied.

The results on the contact surface are determined using ANSYS®'s the contact tool. These data provide detailed information about the distribution of frictional stress and pressure on the elements at the contact surface, which differs from the average values presented in the Bond stress - End displacement curves.

The radial displacement is associated with the negative Poisson's ratio. The results showcased in section 3 are indicated by red to highlight both the positive and null values of radial displacements.

Finally, the results for the safety factor are presented, which represent the Mohr-Coulomb stress safety for brittle materials, calculated using the safety factor tool of ANSYS®. The safety factor is associated with the failure criterion, so values greater than one could indicate potential failure.

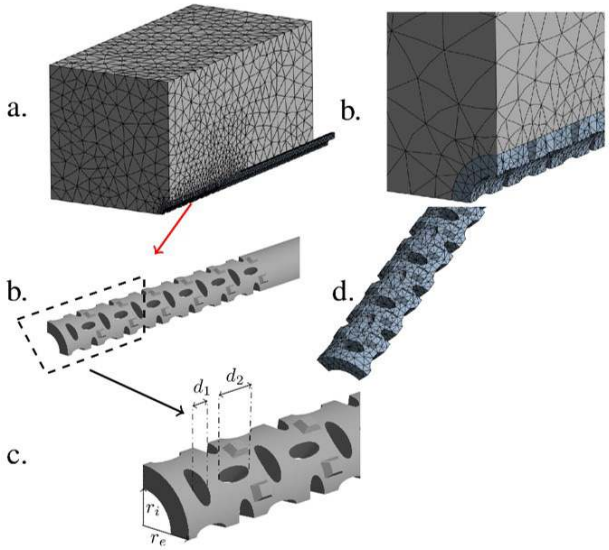


Figure 9. Geometrical model of pull-out test – auxetic example a) 3D view mesh b) 3D mesh ATDR c) ATDR d) ATDR mesh and e) dimensions of ATDR.

3.1 Validation Model – Results

In Figure 10, we compare the simulation conducted in this work using FEM MP with the simulation obtained by Seok et al. (2020) (CDP) and with the experimental data of Kupfer et al. (1969) (Exp). Experimental testing was conducted under load control, ensuring that these data do not extend beyond the onset of strength loss (Seok et al., 2020). Similarly, in our simulations, the numerical data also do not extend beyond this point. The FEM MP responses exhibited similar behavior to the numerical data reported by Seok et al. (2020).

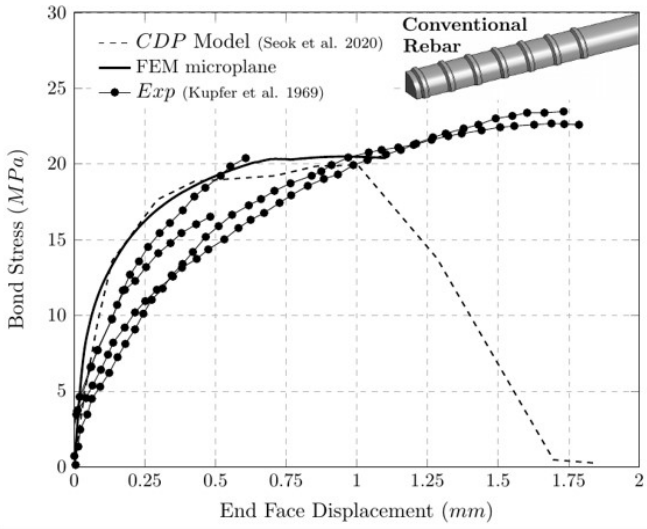


Figure 10. Bond Stress vs. End Face Displacement – Pull-out numerical test for validation.

3.2 TDR and ATDR Models – Results Comparison

As observed in Figure 11, the bond stress versus displacement at the end face (opposite to the face where the displcacement is applied) of the reinforcement bar indicates that the bond stress of ATDR model is higher than that of the TDR model. The comparison between ATDR and TDR models is conducted for two types of concrete, C1 and C2, whith different properties as presented in Table 3. The bonded stress considered average values, following the definition presented in the initial part of section 3, where it is explained that the bond stress is computed as the ratio of the applied force to the contact area between concrete and the rebar. Our initial hypothesis aims to verify whether the auxetic behavior could increase the bond stress between concrete and reinforcement rebar in the Pull-out test by increasing the

normal force on the contact surface. How appreciated in Figure 11, for both concretes, the difference of the bond stress between ATDR e TDR models increases continuously as the rebar's displacement or strain increases. This phenomenon can be explained by the fact that an increase in the normal strain of rebar leads to a higher value of Poisson's ratio. This result, indicated by numerical evidence, suggests that our initial hypothesis could be correct: the auxetic behaviour may increase the bond stress between the concrete and the reinforcement by controlling the normal force on the contact surface, rather than controlling roughness or chemical bonding, as is typically done. In the numerical simulations conducted, the bond stress in the ATDR models was approximately 23% higher for C1 concrete and 19% higher for C2 concrete compared to the TDR models.

The ATDR induces alterations in the distribution of frictional stress and pressure among the elements on the contact surface (the interface between concrete and rebar), as depicted in Figure 12 to Figure 15. These changes are distinct from the average values presented in Figure 10 and Figure 11.

The increase in the normal force is evident in Figure 13 and Figure 15 for C1 and C2 concrete, respectively. These figures show that the pressure (related to the normal force) for ATDR were around 68% and 55% greater than those of TDR models for C1 and C2 concrete, respectively. So, these results show that there is a direct relationship between the increase in normal force, due to the auxetic effect, and the increase in bond stress.

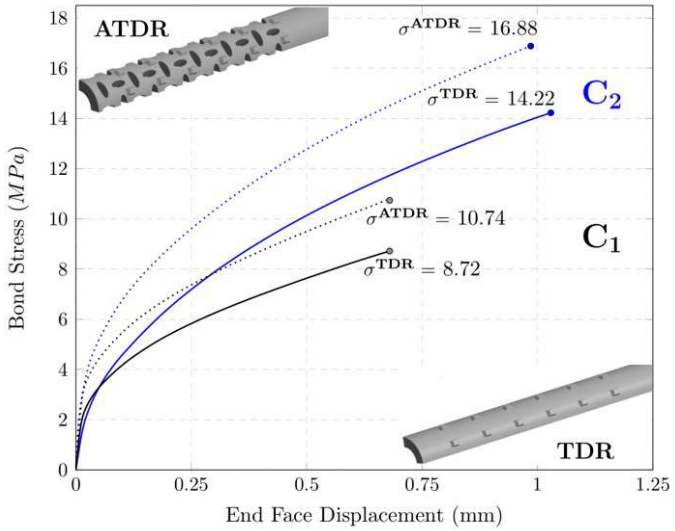


Figure 11. Bond Stress vs. End Face Displacement – Pull-out.

With the maximum values observed, the results indicate that the frictional stress for ATDR models was approximately 54% and 55% higher than that of TDR models for C1 and C2 concrete, respectively.

These findings indeed confirm the potential benefits of employing AMms rebars in concrete structures projects, as they significantly increase the bond stress with the concrete.

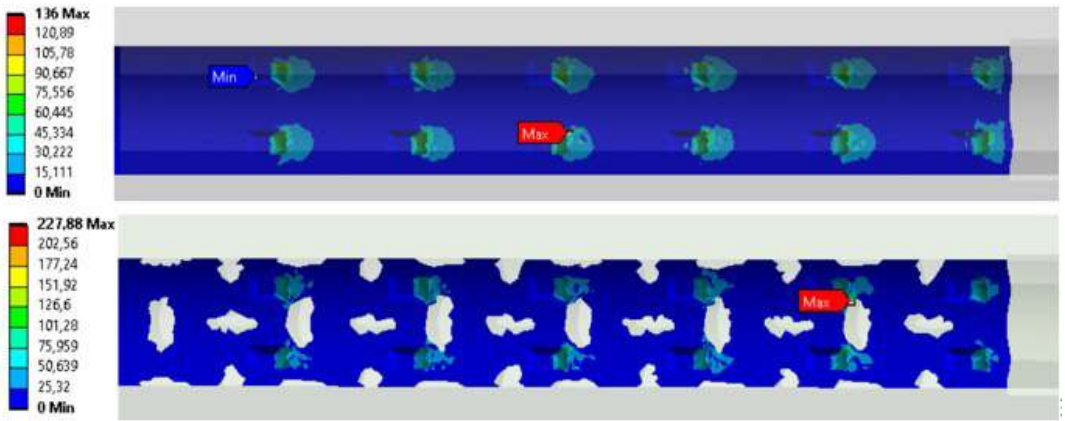


Figure 12. Frictional stress (MPa) on the contact surface with C1 concrete for a) reference model TDR and b) proposed model ATDR.

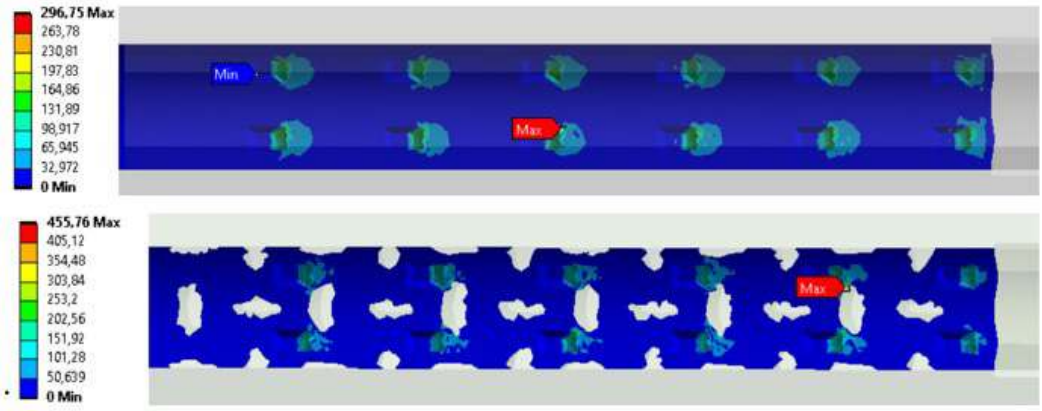


Figure 13. Pressure (MPa) on the contact surface with C1 concrete for a) reference model TDR and b) proposed model ATDR.

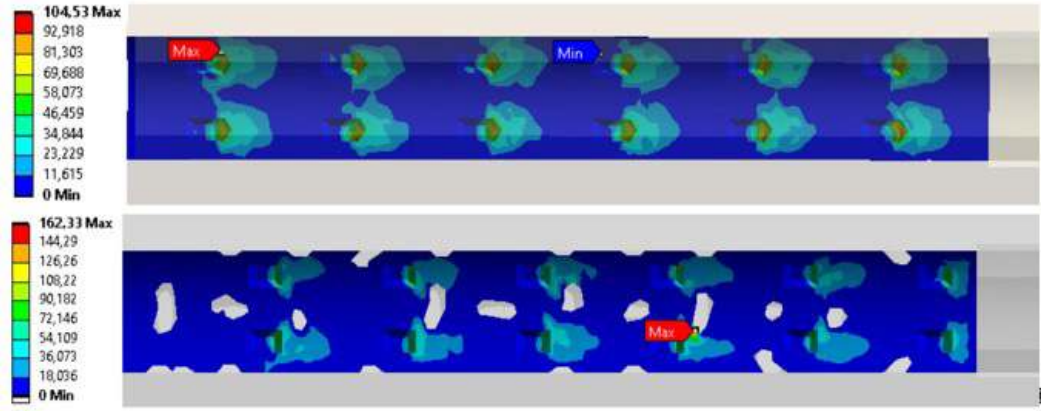


Figure 14. Frictional stress (MPa) on the contact surface with C2 concrete a) reference model TDR and b) proposed model ATDR**.**

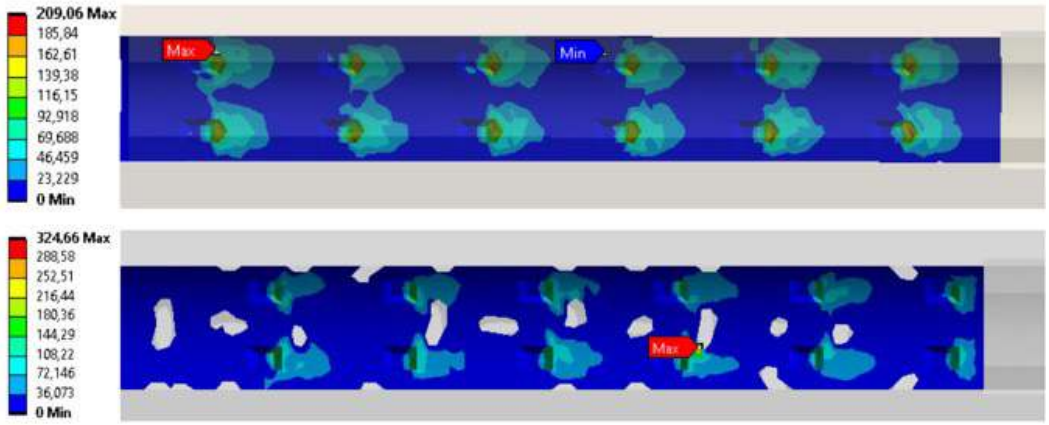


Figure 15. Pressure (MPa) on contact surface with C2 concrete a) reference model TDR and b) proposed model ATDR.

As mentioned in the initial hypothesis, the positive values of radial displacement are associated with the negative Poisson's ratio – non-auxetic behavior. The auxetic behavior, of the initial hypothesis is verified in Figure 16 and Figure 17. While the gain in positive radial displacements obtained for the ATDR bar compared to the TDR bar may seem insignificant when considering absolute values (the change is from -0.00032 in TDR to 0.002988 in ATDR for C1 concrete, and from 0.000246 in TDR to 0.00328 in ATDR for C2 concrete), it is essential to consider the constraint imposed by the concrete block. Therefore, the auxetic behavior is fully verified in the variation of pressure on the contact surface between the concrete and the bars, which is generated by the change in the radial displacement caused by the auxetic effect. Interestingly, for ATDR models, the positive values of radial displacement occur in the same regions as the maximum values of Frictional stress and Pressure on the contact surface (highlighted in red in Figure 16 and Figure 17).

As illustrated in Figure 12 to Figure 15, the maximum values for Frictional stress and Pressure have shifted from the left end in TDR models to the right end (axial direction near to end load) in ATDR models. The total displacement of ATDR, with C1 and C2 concrete, is displayed in Figure 18.

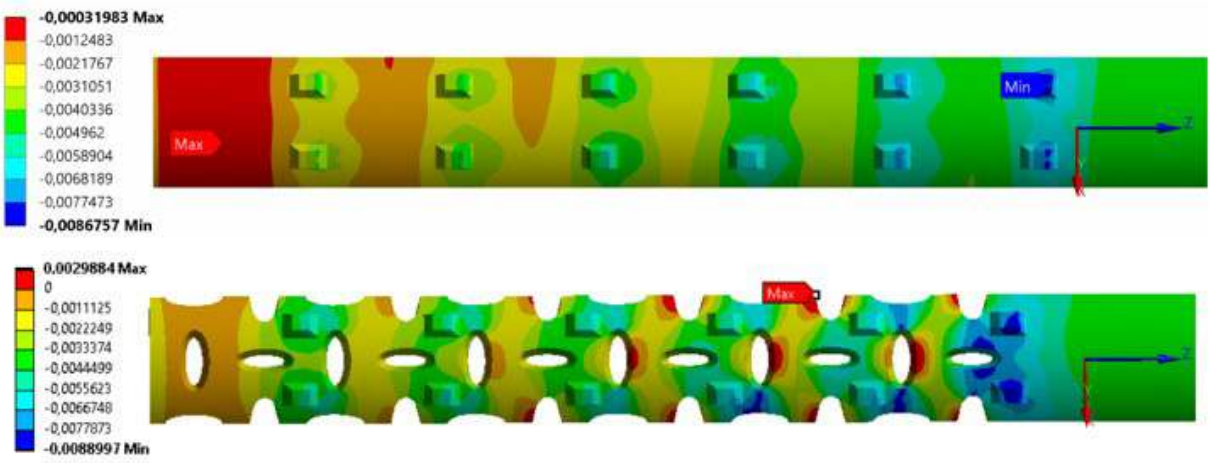


Figure 16. Radial displacement (mm) of rebar with C1 concrete for a) reference model TDR and b) proposed model ATDR

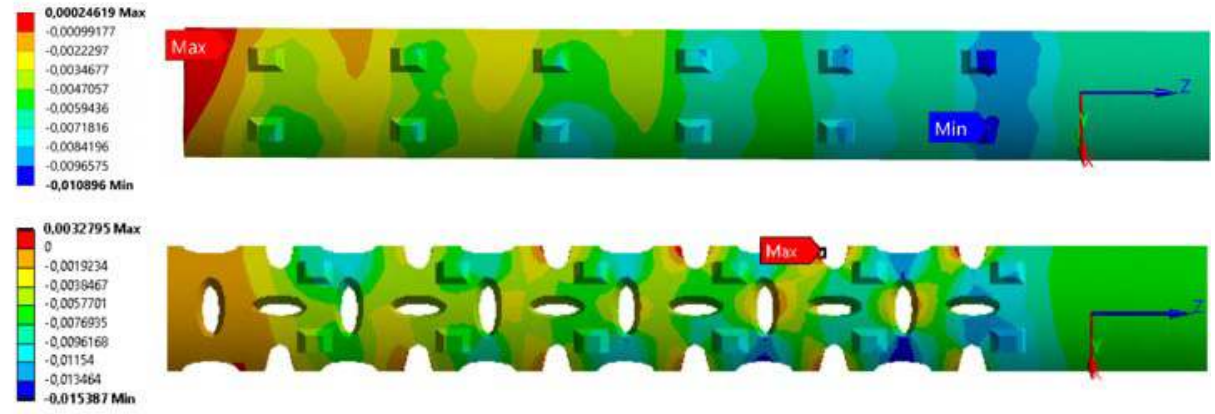


Figure 17. Radial displacement (mm) of rebar with C2 concrete for a) reference model TDR and b) proposed ATDR model.

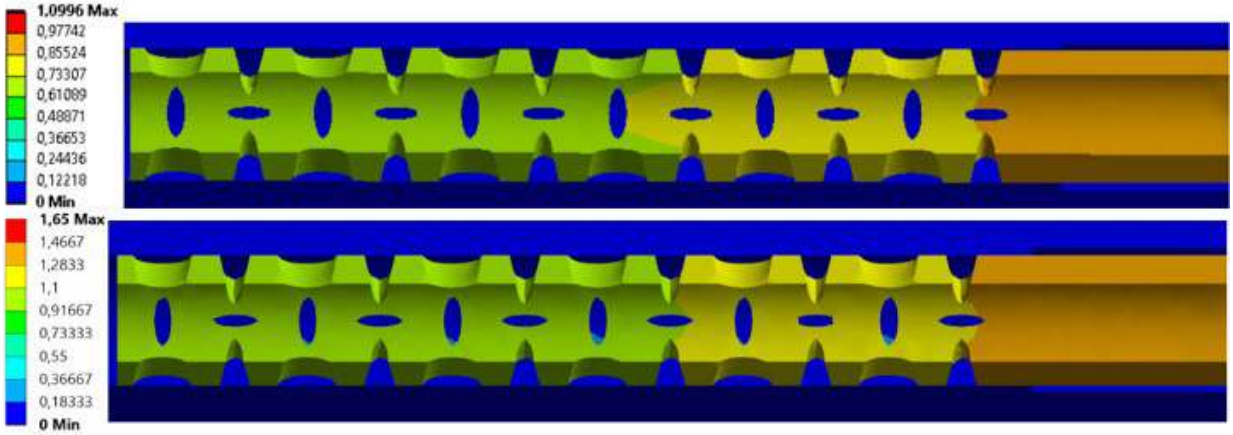


Figure 18. Total displacement (mm) of rebar a) C1 concrete ATDR b) C2 concrete ATDR.

The most noteworthy finding arising from the preceding discussion is that the substantial enhancement in bond strength achievable by incorporating ATDR in the reinforced concrete structures.

4 Conclusions

A novel approach is introduced for reinforcing concrete structures through the utilization of an Auxetic Tubular Deformed Rebar (ATDR). This study employs a HRS FE numerical pull-out test model to assess alterations in bond strength between ATDR and Traditional Deformed Rebar (TDR) while confirming the emergence of negative Poisson's ratio (auxetic behavior) within the reinforced concrete. The numerical methodology underwent validation via two sets of simulations, each conducted with two distinct concrete types, labeled as Ci and C2, characterized by $f_{uc} = 42.7\ MPa$ and $f_{uc} = 28\ MPa$, respectively.

The numerical outcomes concerning the adherence force at the contact surface of ATDR and TDR models, in both C1 and C2 concrete scenarios, revealed a substantial enhancement. Specifically, there was an improvement of 23% and 19% in average bond stress values, along with a remarkable increase of 54% and 55% in frictional stress, and 68% and 55% in pressure. These results unequivocally affirm the practical value of AMms rebars in concrete structures projects.

The most noteworthy conclusion draw from the numerical findings is that incorporation of AMms elements substantially enhances the bond strength of reinforced concrete structures.

Additionally, the obtained results highlight the capability of the microplane (MP) model to accurately capture the behavior of concrete in both compression and tension tests, as well as in pull-out tests. The stress-strain outcomes of the compression and tensile tests reveal that the proposed non-linear FEM MP model, presented in this study, exhibits a significant concurrence with the numerical and experimental data available in the literature. Consequently, the proposed FEM model, featuring a combined plasticity–damage formulation, proves suitable for replicating non-linear response of concrete under various multiaxial stress conditions, particularly during the microcrack state, which results in material softening.

Furthermore, the pull-out numerical test conducted on the reinforced concrete specimens revealed the presence of auxetic radial deformation in the ATDR model. This radial deformation was observed in the C2 concrete models, with a magnitude of $0{,}003\ mm$. Preliminary analysis suggests that the shift in the positions of the maximum values of Frictional stress and Pressure on the contact surface can be attributed to the auxetic behavior of the rebar.

In summary, this work has achieved significant milestones, including the introduction of a novel metareinforcement concept: the 3D ATDR, inspired by metamaterials. This ATDR aims to enhance the adherence force in concrete structures. Additionally, the study has presented a comprehensive numerical methodology utilizing non-linear FEM MP with a HRS approach for reinforced concrete, specifically designed to investigate the mechanical behavior of a new type of auxetic metamaterial (AMm) rebar.

One significant limitation identified in this study is the relatively low auxetic behavior observed in the utilized ATDR geometry. In practical applications, it's important to note that the ATDR model may necessitate a minimum concrete cover to prevent premature cracking and damage in the concrete, similar to the corrosion effect seen in traditional steel rebar. This limitation should be carefully considered in real-world engineering scenarios.

These findings point to several promising avenues for future research: experimental analysis; effects of the auxetic behavior of rebars on the anchorage length in pull-out test; study the behavior of rebars with different auxetic geometries; parametrical analysis of auxetic metamaterial rebars to improve the adherence force or other mechanical properties of auxetic rebars in concrete; the effect of the contact area reduction due to the auxetic geometry on bond stress.

Acknowledgements

This work was carried out within a Metamaterials and Structures group project and was partly sponsored by the National Council for Scientific and Technological Development (CNPq).

Author's Contributions: J.A.G. Sánchez: Project administration, Conceptualization of this study, Supervision, Validation, Data curation, Formal analysis, Investigation, Methodology, Numerical tests, Visualization, Writing – original draft, Writing - review & editing. C.Q. Ramírez: Formal analysis, Investigation, Methodology, Numerical tests, Writing – original draft, Writing - review & editing. P.C. Gonçalves: Formal analysis, Numerical tests, Writing – original draft, Writing - review & editing. O.J. Begambre: Formal analysis, Conceptualization of this study, Writing – original draft, Writing - review & editing.

Editor: Pablo Andrés Muñoz Rojas

References

ANSYS Inc. (2020) 'ANSYS User's Guide'.

Arslan, M.E. and Pul, S. (2020) 'Bond behavior investigation of ordinary concrete-rebar with hinged beam test and eccentric pull-out test', *Computers and Concrete*, 26(6), pp. 587–593. Available at: https://doi.org/10.12989/cac.2020.26.6.587.

Barri, K. et al. (2022) 'Super compressible multifunctional metamaterial concrete', 12043, p. 55. Available at: https://doi.org/10.1117/12.2607689.

Bazant, P.Z. and Pijaudier-Cabot, G. (1989) 'Measurement of characteristic length of nonlocal continuum', *J. Eng. Mech*, 115(4), pp. 755–767.

Bazant, Z.P. et al. (1984) 'Crack Shear in Concree: Crack band Microplane Model', *Struct. Eng.*, 110(9), pp. 2015–2035.

Bazant, Z.P. (1984) 'Microplane Model for Strain-Controlled Inelastic Behaviour.', pp. 45–59.

Bazant, Z.P. and Oh, B.H. (1985) 'Microplane Model for Progressive Fracture of Concrete and Rock', *J. Eng. Mech.*, I(4), pp. 559–582.

Bazant, Z.P. and Ozbolt, J. (1991) 'Nonlocal Microplane Model for Fracture Damage, and Size Effect in Structures', *J. Eng. Mech*, 116(11), pp. 2485–2505.

Benin, A.V. et al. (2013) 'Simulation of degradation of bond between reinforcing bar and concrete. Part 1. Models with account of the discontinuity', *Magazine of Civil Engineering*, 40(5), pp. 86–99. Available at: https://doi.org/10.5862/MCE.40.10.

Benin, A.V. et al. (2014) 'The simulation of bond fracture between reinforcing bars and concrete. Part 2', *Magazine of Civil Engineering*, 1, pp. 20–25.

Bertoldi, K. et al. (2017) 'Flexible mechanical metamaterials', *Nature Reviews Materials*, 2. Available at: https://doi.org/10.1038/natrevmats.2017.66.

Brisotto, D.D.S., Bittencourt, E. and Bessa, V.M.R.D.A. (2012) 'Simulating bond failure in reinforced concrete by a plasticity model', *Computers and Structures*, 106–107, pp. 81–90. Available at: https://doi.org/10.1016/j.compstruc.2012.04.009.

Brocca, M. and Bažant, Z.P. (2000) 'Microplane constitutive model and metal plasticity', *Applied Mechanics Reviews*, 53(10), pp. 265–281. Available at: https://doi.org/10.1115/1.3097329.

Carol, B.I. et al. (1991) 'Geometric damage tensor based on microplane model', *J. Eng. Mech.*, 117(10), pp. 2429–2448.

Comi, C. and Driemeier, L. (2018) 'Wave propagation in cellular locally resonant metamaterials', *Latin American Journal of Solids and Structures*, 15(4). Available at: https://doi.org/10.1590/1679-78254327.

Erfanian, A. and Elwi, A.E. (2019) 'Bond Plastic Model for Steel–Concrete Damaged Interface Element', *Journal of Structural Engineering*, 145(5), p. 04019018. Available at: https://doi.org/10.1061/(asce)st.1943-541x.0002302.

Fabbrocino, F. et al. (2016) 'Optimal design and additive manufacturing of novel reinforcing elements for composite materials', *ECCOMAS Congress 2016 - Proceedings of the 7th European Congress on Computational Methods in Applied Sciences and Engineering*, 1(April 2017), pp. 1893–1908. Available at: https://doi.org/10.7712/100016.1928.4544.

Farina, I et al. (2016a) 'On the reinforcement of cement mortars through 3D printed polymeric and metallic fi bers', *Composites Part B*, 90, pp. 76–85. Available at: https://doi.org/10.1016/j.compositesb.2015.12.006.

Farina, Ilenia et al. (2016b) 'Surface roughness effects on the reinforcement of cement mortars through 3D printed metallic fibers', *Composites Part B: Engineering*, 99, pp. 305–311. Available at: https://doi.org/10.1016/j.compositesb.2016.05.055.

Fleck, N.A., Deshpande, V.S. and Ashby, M.F. (2010) 'Micro-architectured materials: Past, present and future', *Proceedings of the Royal Society A: Mathematical, Physical and Engineering Sciences*, 466(2121), pp. 2495–2516. Available at: https://doi.org/10.1098/rspa.2010.0215.

Fraternali, F. et al. (2015) 'On the use of mechanical metamaterials for innovative seismic isolation systems', in *5th ECCOMAS Thematic Conference on Computational Methods in Structural Dynamics and Earthquake Engineering*. Greece, pp. 349–358. Available at: https://doi.org/10.7712/120115.3401.636.

Friedrich, L.F. and Wang, C. (2016) 'Continuous modeling technique of fiber pullout from a cement matrix with different interface mechanical properties using finite element program', *Latin American Journal of Solids and Structures*, 13(10), pp. 1937–1953. Available at: https://doi.org/10.1590/1679-78252575.

Gao, J. et al. (2019) 'Topology optimization for auxetic metamaterials based on isogeometric analysis', *Computer Methods in Applied Mechanics and Engineering*, 352, pp. 211–236. Available at: https://doi.org/10.1016/j.cma.2019.04.021.

Gonçalves Salsa Junior, R., de Paula Sales, T. and Rade, D. (2022) 'Optimization of Vibration Band Gaps in Damped Elastic Metamaterials', 20(6), pp. 1–20. Available at: https://doi.org/10.26678/abcmhttps://doi.org/10.1590/1679-78257486mecsol2022.msl22-0014.

Grassl, P. and Jirásek, M. (2006a) 'Damage-plastic model for concrete failure', *International Journal of Solids and Structures*, 43(22–23), pp. 7166–7196. Available at: https://doi.org/10.1016/j.ijsolstr.2006.06.032.

Grassl, P. and Jirásek, M. (2006b) 'Plastic model with non-local damage applied to concrete', *International Journal for Numerical and Analytical Methods in Geomechanics*, 30(1), pp. 71–90. Available at: https://doi.org/10.1002/nag.479.

Guevara-Corzo, J.J. et al. (2022) 'Passive seismic protection systems with mechanical metamaterials: A current review', *Structural Engineering and Mechanics*, 82(4), pp. 417–434. Available at: https://doi.org/10.12989/sem.2022.82.4.417.

Gupta, A. et al. (2023) 'Metamaterial foundation for seismic wave attenuation for low and wide frequency band', *Scientific Reports*, 13(1), pp. 1–14. Available at: https://doi.org/10.1038/s41598-023-27678-1.

Hou, S. et al. (2018) 'Mechanical properties of sandwich composites with 3d-printed auxetic and non-auxetic lattice cores under low velocity impact', *Materials and Design*, 160, pp. 1305–1321. Available at: https://doi.org/10.1016/j.matdes.2018.11.002.

Indriyantho, B.R., Zreid, I. and Kaliske, M. (2019) 'Finite strain extension of a gradient enhanced microplane damage model for concrete at static and dynamic loading', *Engineering Fracture Mechanics*, 216(February), p. 106501. Available at: https://doi.org/10.1016/j.engfracmech.2019.106501.

Indriyantho, B.R., Zreid, I. and Kaliske, M. (2020) 'A nonlocal softening plasticity based on microplane theory for concrete at finite strains', *Computers and Structures*, 241, p. 106333. Available at: https://doi.org/10.1016/j.compstruc.2020.106333.

Jagiello, E. and Muñoz-Rojas, P.A. (2021) 'An extended multiscale finite element method (Emsfem) analysis of periodic truss metamaterials (ptmm) designed by asymptotic homogenization', *Latin American Journal of Solids and Structures*, 18(2), pp. 1–30. Available at: https://doi.org/10.1590/1679-78256240.

Jeeho Lee and Gregory L. Fenves (1998) 'Plastic-Damage Model for Cyclic Loading of Concrete Structures', *Journal of Engineering Mechanics*, 124(8), pp. 892–900.

Jiang, H. and Zhao, J. (2015) 'Calibration of the continuous surface cap model for concrete', *Finite Elements in Analysis and Design*, 97, pp. 1–19. Available at: https://doi.org/10.1016/j.finel.2014.12.002.

Kuhl, E., Ramm, E. and De Borst, R. (2000) 'An anisotropic gradient damage model for quasi-brittle materials', *Computer Methods in Applied Mechanics and Engineering*, 183(1–2), pp. 87–103. Available at: https://doi.org/10.1016/S0045-7825(99)00213-3.

Kupfer, H., Hilsdorf, H.K. and Rusch, H. (1969) 'Behavior of Concrete Under Biaxial Stresses', *Journal Proceedings*, 66.

Leukart, M. and Ramm, E. (2003) 'A comparison of damage models formulated on different material scales', *Computational Materials Science*, 28(3-4 SPEC. ISS.), pp. 749–762. Available at: https://doi.org/10.1016/j.commatsci.2003.08.029.

Leukart, M. and Ramm, E. (2006) 'Identification and Interpretation of Microplane Material Laws', *Journal of Engineering Mechanics*, 132(3), pp. 295–305. Available at: https://doi.org/10.1061/(asce)0733-9399(2006)132:3(295).

Li, J., Tue, N. V. and Caner, F.C. (2013) 'Microplane constitutive model M4L for concrete. II: Calibration and validation', *Computers and Structures*, 128, pp. 146–159. Available at: https://doi.org/10.1016/j.compstruc.2013.06.009.

Li, T. et al. (2017) 'Harnessing out-of-plane deformation to design 3D architected lattice metamaterials with tunable Poisson's ratio', *Scientific Reports*, 7(1), pp. 1–10. Available at: https://doi.org/10.1038/s41598-017-09218-w.

Liang, J.-F. et al. (2017) 'Bond behavior between high volume fly ash concrete and steel rebars', *Computers and Concrete*, 19(9), pp. 625–630. Available at: https://doi.org/10.12989/cac.2017.19.6.625.

Liang, J. et al. (2021) 'Bond behavior of FRP bars in CR concrete', *Computers and Concrete*, 28(2), pp. 107–114. Available at: https://doi.org/10.12989/cac.2021.28.2.107.

Lundgren, K. (2005a) 'Bond between ribbed bars and concrete. Part 1: Modified model', *Magazine of Concrete Research*, 57(7), pp. 371–382. Available at: https://doi.org/10.1680/macr.2005.57.7.371.

Lundgren, K. (2005b) 'Bond between ribbed bars and concrete. Part 2: The effect of corrosion', *Magazine of Concrete Research*, 57(7), pp. 383–395. Available at: https://doi.org/10.1680/macr.2005.57.7.383.

Lundgren, K. and Gylltoft, K. (2000) 'Model for the bond between concrete and reinforcement', *Magazine of Concrete Research*, 52(1), pp. 53–63. Available at: https://doi.org/10.1680/macr.2000.52.1.53.Luo, C. et al. (2021) 'Design, manufacturing and applications of auxetic tubular structures: A review', Thin-Walled Structures, 163(December 2020). Available at: https://doi.org/10.1016/j.tws.2021.107682

De Maio, U. et al. (2019) 'A study of concrete cover separation failure in FRP-plated RC beams via an inter-element fracture approach', *Composite Structures*, 212(January), pp. 625–636. Available at: https://doi.org/10.1016/j.compstruct.2019.01.025.

Martinsson, P.G. and Babuška, I. (2007) 'Mechanics of materials with periodic truss or frame micro-structures', *Archive for Rational Mechanics and Analysis*, 185(2), pp. 201–234. Available at: https://doi.org/10.1007/s00205-006-0044-2.

Miranda, M.P. et al. (2021) 'Steel-concrete bond behavior: An experimental and numerical study', *Construction and Building Materials*, 271, p. 121918. Available at: https://doi.org/10.1016/j.conbuildmat.2020.121918.

Mitchell, S.J., Pandolfi, A. and Ortiz, M. (2014) 'Metaconcrete: Designed aggregates to enhance dynamic performance', *Journal of the Mechanics and Physics of Solids*, 65(1), pp. 69–81. Available at: https://doi.org/10.1016/j.jmps.2014.01.003.

Mitchell, S.J., Pandolfi, A. and Ortiz, M. (2015) 'Investigation of elastic wave transmission in a metaconcrete slab', *Mechanics of Materials*, 91(P1), pp. 295–303. Available at: https://doi.org/10.1016/j.mechmat.2015.08.004.

Nolan C. Concha and Oreta, A.W.C. (2021) 'Investigation of the effects of corrosion on bond strength of steel in concrete using neural network', *Computers and Concrete*, 28(1), pp. 77–91. Available at: https://doi.org/10.12989/cac.2021.28.1.077.

Qasem, A. et al. (2020) 'Bond-slip behavior between ultra-high-performance concrete and carbon fiber reinforced polymer bars using a pull-out test and numerical modelling', *Construction and Building Materials*, 260, p. 119857. Available at: https://doi.org/10.1016/j.conbuildmat.2020.119857.

Ramírez, C.Q. et al. (2022) 'Interfacial Bonding Strength in Cement Mortar Beams Reinforced with Metamaterial Bars', *Materials Research*, 25. Available at: https://doi.org/10.1590/1980-5373-MR-2021-0383.

Ren, X., Das, R., et al. (2018a) 'Auxetic metamaterials and structures: A review', *Smart Materials and Structures*, 27(2). Available at: https://doi.org/10.1088/1361-665X/aaa61c.

Ren, X., Shen, J., et al. (2018b) 'Auxetic nail: Design and experimental study', *Composite Structures*, 184(July 2017), pp. 288–298. Available at: https://doi.org/10.1016/j.compstruct.2017.10.013.

Rodrigues, G.K., Da Silva, M.M. and De Oliveira, L.P.R. (2019) 'Modular modeling approach for FDM printed structures and piezo disks for metamaterial design', Latin American Journal of Solids and Structures, 16(7 CILAMCE 2018), pp. 1–14. Available at: https://doi.org/10.1590/1679-78255310.

Salem, H.M. and Maekawa, K. (2004) 'Pre- and Postyield Finite Element Method Simulation of Bond of Ribbed Reinforcing Bars', *Journal of Structural Engineering*, 130(4), pp. 671–680. Available at: https://doi.org/10.1061/(asce)0733-9445(2004)130:4(671).

Schreter, M., Neuner, M. and Hofstetter, G. (2018) 'Evaluation of the implicit gradient-enhanced regularization of a damage-plasticity rock model', *Applied Sciences (Switzerland)*, 8(6). Available at: https://doi.org/10.3390/app8061004.

Schwer, L.E. and Murray, Y.D. (1994) 'A three-invariant smooth cap model with mixed hardening', *International Journal for Numerical and Analytical Methods in Geomechanics*, 18(10), pp. 657–688. Available at: https://doi.org/10.1002/nag.1610181002.

Seok, S. (2019) *Finite Element Modeling of Bond-Zone Behavior in Reinforced Concrete.* Purdue University.

Seok, S. et al. (2020) 'Finite element simulation of bond-zone behavior of pullout test of reinforcement embedded in concrete using concrete damage-plasticity model 2 (CDPM2)', *Engineering Structures*, 221(May), p. 110984. Available at: https://doi.org/10.1016/j.engstruct.2020.110984.

Song, J. et al. (2020) 'Experimental study on the bond-slip performance between concrete and a corrugated steel plate with studs', *Engineering Structures*, 224(June), p. 111195. Available at: https://doi.org/10.1016/j.engstruct.2020.111195.

Steinke, C., Zreid, I. and Kaliske, M. (2017) 'On the relation between phase-field crack approximation and gradient damage modelling', *Computational Mechanics*, 59(5), pp. 717–735. Available at: https://doi.org/10.1007/s00466-016-1369-9.

Tang, C.W. (2015) 'Local bond stress-slip behavior of reinforcing bars embedded in lightweight aggregate concrete', *Computers and Concrete*, 16(3), pp. 449–466. Available at: https://doi.org/10.12989/cac.2015.16.3.449.

Tran, M.T., Vu, X.H. and Ferrier, E. (2021) 'Experimental and numerical investigation of carbon textile/cementitious matrix interfacebehaviourfrom pull-out tests', *Construction and Building Materials*, 282, p. 122634. Available at: https://doi.org/10.1016/j.conbuildmat.2021.122634.

Xenos, D. et al. (2015) 'Calibration of nonlocal models for tensile fracture in quasi-brittle heterogeneous materials', *Journal of the Mechanics and Physics of Solids*, 82, pp. 48–60. Available at: https://doi.org/10.1016/j.jmps.2015.05.019.

Xianglong, Y. et al. (2018) 'Mechanical metamaterials associated wit...ty and compressibility_ A brief review.pdf', *Progress in Materials Science*, 94, pp. 114–173.

Zdenek P. Bazant and Prat, P.C. (1989) 'Microplane model for brittle-plastic material: I. Theory', *J. Eng. Mech.*, 114(10), pp. 1672–1688.

Zhang, G. and Khandelwal, K. (2019) 'Computational design of finite strain auxetic metamaterials via topology optimization and nonlinear homogenization', *Computer Methods in Applied Mechanics and Engineering*, 356, pp. 490–527. Available at: https://doi.org/10.1016/j.cma.2019.07.027.Zhang, J., Lu, G. and You, Z. (2020) 'Large deformation and energy absorption of additively manufactured auxetic materials and structures: A review', Composites Part B: Engineering, 201, pp. 1–90. Available at: https://doi.org/10.1016/j.compositesb.2020.108340

Zhong, R. et al. (2022) 'Mechanical properties of concrete composites with auxetic single and layered honeycomb structures', *Construction and Building Materials*, 322(August 2021), p. 126453. Available at: https://doi.org/10.1016/j.conbuildmat.2022.126453.

Zreid, I. and Kaliske, M. (2016a) 'An implicit gradient formulation for microplane Drucker-Prager plasticity', *International Journal of Plasticity*, 83, pp. 252–272. Available at: https://doi.org/10.1016/j.ijplas.2016.04.013.

Zreid, I. and Kaliske, M. (2016b) 'An implicit gradient formulation for microplane Drucker-Prager plasticity', *International Journal of Plasticity*, 83, pp. 252–272. Available at: https://doi.org/10.1016/j.ijplas.2016.04.013.

Zreid, I. and Kaliske, M. (2018) 'A gradient enhanced plasticity–damage microplane model for concrete', *Computational Mechanics*, 62(5), pp. 1239–1257. Available at: https://doi.org/10.1007/s00466-018-1561-1.